Bull Earthquake Eng (2017) 15:3437–3461
DOI 10.1007/s10518-017-0122-x

ORIGINAL RESEARCH PAPER

A ground motion prediction equation for novel peak ground fractional order response intensity measures

Özkan Kale[1] · Jamie E. Padgett[2] · Abdollah Shafieezadeh[3]

Received: 22 August 2016 / Accepted: 11 March 2017 / Published online: 17 March 2017

Abstract Peak ground fractional order responses (PGR_α) as a generalization of conventional seismic intensity measures (IMs) such as peak ground acceleration (PGA) and peak ground velocity (PGV) can better predict the seismic performance of structural systems. This paper proposes the first ground motion prediction equation (GMPE) for PGR_α for active shallow crustal regions using a subset of the PEER NGA-West2 ground motion database. The model development database consists of 4491 accelerograms from 82 different earthquakes in California with the magnitude and rupture distance ranges of M_w 4.0–7.9 and R_{RUP} 0–300 km, respectively. PGR_α intensity measures are computed from the modified Oustaloup's recursive approximation to Caputo's definition of differintegral operator. The main functional form of the predictive model is decided by implementing statistical ground motion data-driven testing methods such as the likelihood approach and Euclidean distance concept. The final functional form of the predictive model accounts for magnitude, distance, style-of-faulting, linear and nonlinear site, hanging wall, basin response, and anelastic distance attenuation effects, and models the aleatory variability with respect to M_w and V_{S30}. The final predictive model produces PGA ($\alpha = 0$), PGV ($\alpha = -1$), and peak ground fractional order responses at 19 different α values ranging from -0.05 to -0.95 for the average horizontal component. The proposed predictive model draws estimates of ground motion amplitudes that are consistent with those from the NGA-West2 models for PGA and PGV for sample earthquake scenarios. Moreover, it can

Electronic supplementary material The online version of this article (doi:10.1007/s10518-017-0122-x) contains supplementary material, which is available to authorized users.

✉ Özkan Kale
ozkankale@gmail.com

[1] Department of Civil Engineering, TED University, Ziya Gökalp Cad. No: 48, 06420 Çankaya, Ankara, Turkey

[2] Department of Civil and Environmental Engineering, Rice University, 6100 Main St., MS-318, Houston, TX 77005, USA

[3] Department of Civil, Environmental, and Geodetic Engineering, The Ohio State University, 470 Hitchcock Hall, 2070 Neil Ave, Columbus, OH 43210, USA

offer a basis for predictive modeling of peak ground fractional order response quantities for performance assessment of structures and infrastructures across a region.

Keywords Peak ground fractional response · Seismic intensity measure · Ground motion prediction equation · Seismic risk assessment · Infrastructure vulnerability

1 Introduction

Two key ingredients for seismic risk assessment are probabilistic seismic demand models (PSDMs) relating the response of a structural system, or infrastructure component, to a parameter representing the strength of earthquake events called the seismic intensity measure (IM), and the corresponding ground motion prediction equations (GMPEs) characterizing the probability model of the IM. The IMs selected to characterize the earthquake intensity and predict seismic behavior play a critical role in affecting the uncertainty propagated in the risk assessment and loss estimation framework (Mackie and Stojadinovic 2001, 2004; Shafieezadeh et al. 2012; Padgett et al. 2008; Luco and Cornell 2007). To predict infrastructure performance, the current practice of adopting hazard intensity measures based on integer order derivatives or integrals of the ground motion time history (e.g. peak ground acceleration or spectral acceleration) may not be efficient. Complex dynamic features of key infrastructure constituents under earthquake loads may not be optimally predicted using discrete states of acceleration, velocity, or displacement sensitivities which are the basis for the set of traditional earthquake IMs used in seismic risk assessment. Large levels of uncertainties in probabilistic models that predict both ground motion IMs and the associated physical response of structural systems induce significant uncertainties in the final outcome of risk analyses. This uncertainty can undermine confidence in the resulting risk estimates, and pose a significant challenge in implementing such methods for risk-informed decision making purposes.

A new perspective on characterizing earthquake intensity for modeling seismic risk to distributed infrastructure systems is required to enable robust analytical methods for reliable probabilistic characterization of earthquakes across a region, efficient modeling of the physical demand imparted on infrastructures, and increased confidence in resulting risk estimates. The introduction of fractional order calculus to uncover so-called "α-order" ground motion intensity can offer the basis of this transformation. Extending the integer order of differential operators (derivative and integral) to arbitrary real numbers in the context of fractional order calculus releases a major limitation of classical probabilistic and mechanistic modeling which has found applications in various fields of science and engineering such as visco-elastic material modeling (Müller et al. 2011; Mainardi 2010; Meral et al. 2010), control of dynamical systems (Li et al. 2010a, b; Monje et al. 2010; Tavazoei and Haeri 2008; Caponetto 2010; Odibat 2010) and structural engineering (Ruge and Trinks 2004). Several studies have introduced fractional order calculus within the domain of earthquake engineering, for example to model the response of structures with damping or isolation systems (Koh and Kelly 1990; Chang and Singh 2002; Singh et al. 2011), or to characterize the viscoelastic behavior of soils in the presence of seismic waves (Dikmen 2005; Lenti et al. 2012). Experimental studies by Oldham and Spanier (1974) revealed that the damping behavior of some materials in the frequency domain follows a power law model with non-integer orders. Gaul et al. (1991) in a study on simulation of

wave propagation in soil domains showed that the frequency domain behavior of visco-elastic soil materials can be better described using fractional order models compared to conventional integer order models. Considering soil medium as a system responsible for propagation of waves from source to the surface, given the above noted fractional characteristics, it is expected that the outputs of the system i.e. ground motions at the surface and responses of structures to these excitations will have fractional order characteristics as well. Shafieezadeh et al. (2012) leveraged this feature and developed a series of fractional order intensity measures by primarily releasing the constraints of integer orders in conventional IMs. The performance of these IMs were evaluated against conventional intensity measures for a class of bridges that accounts for about 20% of the bridge inventory in the state of California. Results indicated that fractional order IMs can significantly reduce dispersions in probabilistic seismic demand models for engineering demand parameters of interest by as much as 36% compared to conventional IMs. In short, fractional order IMs can offer good predictive quality of structural response while reducing uncertainty introduced into the probabilistic analysis.

The study by Shafieezadeh et al. (2012) reveals the fact that there is a strong need for developing fractional order GMPEs because site-specific or regional seismic hazard analyses are required in order for fractional order IMs to be usable in practice. To do so, this paper proposes the first GMPE for estimating peak ground fractional order response (PGR_α) IMs. In this respect, a ground-motion database is compiled from the PEER NGA-West2 project database (Ancheta et al. 2014) for developing the PGR_α predictive model which is mainly appropriate for active shallow crustal earthquakes in California. Next, the PGR_α earthquake intensities of the recordings in the ground-motion database are computed by utilizing a fractional order numerical approximation approach. The PGR_α predictive model at peak ground acceleration (PGA; $\alpha = 0$), peak ground velocity (PGV; $\alpha = -1$) and various α values (between 0 and -1) are then derived by accounting for magnitude, distance, style-of-faulting, linear and nonlinear site, hanging wall, basin response, and anelastic distance attenuation effects in the ground-motion estimates. The proposed GMPE models the aleatory variability (i.e., standard deviation) by taking into account the magnitude and nonlinear site effects that provide more accurate realizations of the ground motion estimates.

2 Peak ground fractional order response IMs

In the literature, various definitions of fractional order operators have been proposed; among which the Grunwald–Letnikov, Riemann–Liouville, and Caputo's definitions are widely used formulations for fractional order derivation and integration (Podlubny 1999). However, Caputo's definition is the most preferred one in engineering applications because it gives bounded values for fractional derivatives of constants and includes physically interpretable initial conditions such as displacement and velocity. Based on Caputo's definition, the α-derivative of a function $f(t)$ defined on the interval [0, T] at time $t \in (0, T]$ can be expressed in the form of a convolution integral as shown in Eq. (1). In this equation, ${}_0^C D_t^\alpha$ denotes the notion of the Caputo's (i.e. C) differintegral fractional operator of a real valued order α with respect to the variable t, starting at time $t = t_0 = 0$ whereas p is an integer number that satisfies $p-1 < \alpha \leq p$ and $\Gamma(*)$ is Euler's Gamma function.

$$ {}_0^C D_t^{\alpha} f(t) = \begin{cases} \dfrac{1}{\Gamma(\alpha - p)} \displaystyle\int_0^t \dfrac{f(\tau)^p}{(t-\tau)^{\alpha+1-p}} d\tau; & \alpha \geq 0 \\ \dfrac{1}{\Gamma(-\alpha)} \displaystyle\int_0^t \dfrac{f(\tau)}{(t-\tau)^{\alpha+1}} d\tau; & \alpha < 0 \end{cases} \quad (1) $$

The limitation of integer order derivatives of ground displacement can be released by taking the α-order integral of ground acceleration ($\ddot{x}_g$) and presenting peak ground fractional order response (PGR_α) as:

$$ PGR_\alpha = \max_0^T \left(\left| {}_0^C D_t^{\alpha} \ddot{x}_g(t) \right| \right) \quad (2) $$

Among the various techniques that have been proposed for numerical realization of fractional order derivatives and integrals, the modified approach for Oustaloup recursive approximation to Caputo derivatives in the frequency domain (Oustaloup et al. 2000; Xue et al. 2006) is adopted given its accuracy at a reasonable computation time. The reader is referred to Shafieezadeh et al. (2012) for the details of this approximation, which is integrated in the SIMULINK environment of MATLAB (MathWorks 2015) and used for computing PGR_α values herein. Illustrations of the application of the modified Oustaloup approximation technique to couple of accelerograms (M_w 6.69 Northridge Earthquake of 01/17/1994, Beverly Hills-14145 Mulhol Station, MUL009 horizontal component and M_w 4.27 Yorba Linda Earthquake of 09/03/2002, LA—Obregon Park Station, 24400360 horizontal component) are shown in Fig. 1. Results for PGR_α are compared with conventional peak ground motion IMs for integer values of α. The results show the agreement of the approximated α-order IMs using the modified Oustaloup method with the traditional IMs computed from the accelerograms, and reinforce the definitions of α-order IMs at integer orders (e.g. PGA, PGV and PGD). They also illustrate the trend regarding variation of PGR with α for the selected motions.

Figure 2 shows another illustration for the first recording (Northridge Earthquake) to give a slight intuition about the physical interpretation of these IMs. The time series of the

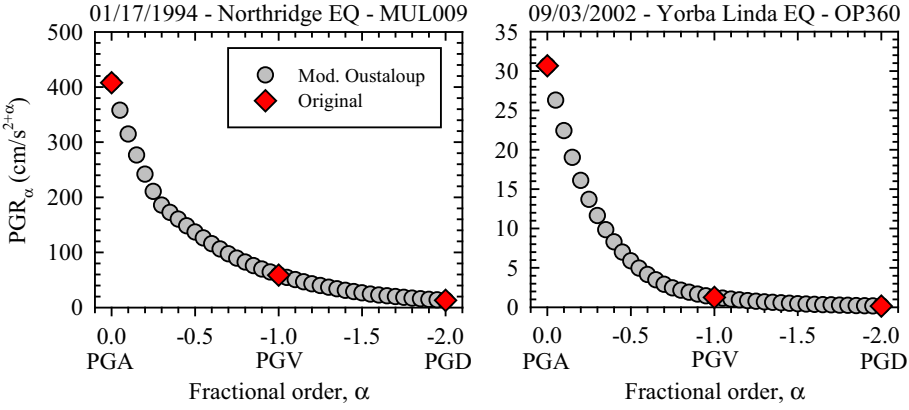

Fig. 1 Comparison of approximated PGR_α values with conventional peak ground motion IMs

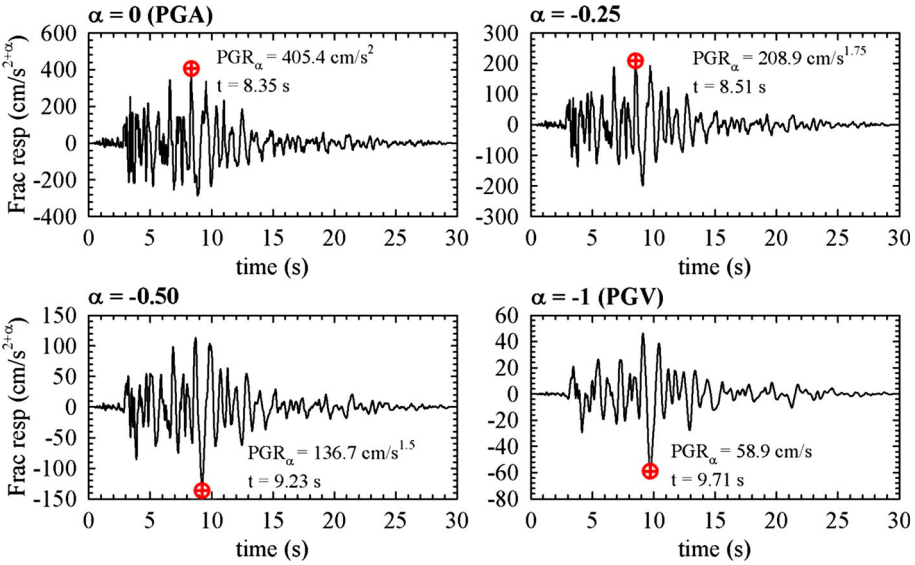

Fig. 2 Comparison of approximated PGR_α values with conventional peak ground motion IMs

ground motion recording for different alpha levels [i.e. alpha = 0 (PGA), −0.25, −0.50, −1 (PGV)] is shown in this figure. The observation made from this figure is that the time-step at which the peak ground fractional responses occur do not coincide with the time step of conventional peak ground responses (i.e. PGA and PGV). This indicates that the peak ground fractional responses are related to the different frequency content of the ground motion data.

3 Ground motion database

The ground-motion database utilized in this study is a subset of the PEER NGA-West2 database (Ancheta et al. 2014) which was compiled from the worldwide recordings of shallow active crustal regions (e.g. California, Italy, Turkey, Japan, China, etc.). The subset of expanded PEER NGA-West2 database is extracted by considering inclusion criteria comparable to those in Campbell and Bozorgnia (2014). The selected events are mainshock earthquakes from the Western United States (US) with moment magnitude $M_w \geq 4.0$ and extended-source distance metrics Joyner-Boore (R_{JB}) ≤ 300 km and rupture (R_{RUP}) - ≤ 300 km. Another selection criterion is the presence of known style-of-faulting information based on rake angles and measured or inferred values of V_{S30}-based site classes of the strong motion stations. Only good quality recordings (e.g. spectral shape, well-triggered, and free field) are included in the database. In addition, a filter is applied to the events in order to select only well-recorded earthquakes with respect to minimum number of recordings (N) criteria: $N < 5$ for $M_w < 5.5$, $N < 3$ for $5.5 \leq M_w < 6.5$. A number of additional accelerograms that potentially satisfy the above set of criteria were not included in the database because of systematic problems downloading them from the PEER ground motion database.

The application of the aforementioned criteria results in compilation of a ground-motion database with the total number of 4491 recordings from 82 earthquakes and 1366 strong

motion stations. In the final database, 2366 accelerograms recorded from 73 earthquakes can be classified as near-source ground motion following the criterion of R_{JB} and $R_{RUP} < 80$ km. This threshold can be considered as a limit for earthquakes to have significance in probabilistic seismic hazard analysis and structural engineering applications. ESM_1.1 lists the details of ground motion database in terms of selected earthquakes, recording sites and distance classes.

The distribution of R_{RUP} versus M_w along with their individual distributions for the ground motions in the database are shown in Fig. 3. There are sufficient data to model the magnitude effects in the predictive model except for the very largest magnitude bin ($M_w > 7.5$) and partially one of the moderate magnitude bins ($6.0 < M_w < 6.5$). The extent of data for the close distance range (i.e. $R_{RUP} < 20$ km) is less than that for the rest of distance ranges in the database but the number of recordings is sufficient to satisfactorily model the distance effects in the GMPE.

Figure 4 displays the R_{RUP} versus M_w distribution of ground motion data with respect to style-of-faulting (strike-slip-SS; normal-NM; reverse-RV) and site class. The National Earthquake Hazards Reduction Program (NEHRP; Building Seismic Safety Council [BSSC], 2009) site classification is used in the comparative plots. The SS and RV ground motion data are well represented in the database, whereas the database lacks a sufficient number of accelerograms from NM faulting earthquakes; however, NM faulting earthquakes are not characteristic of the regional seismicity. The database includes measured and inferred V_{S30} values for NEHRP site classifications and for modeling the linear and nonlinear site effects of the predictive model. A significant amount of data in the database is coming from strong-motion stations located on the NEHRP-C and -D site categories (Fig. 5). Beyond this, an adequate number of rock site accelerograms are included in the database.

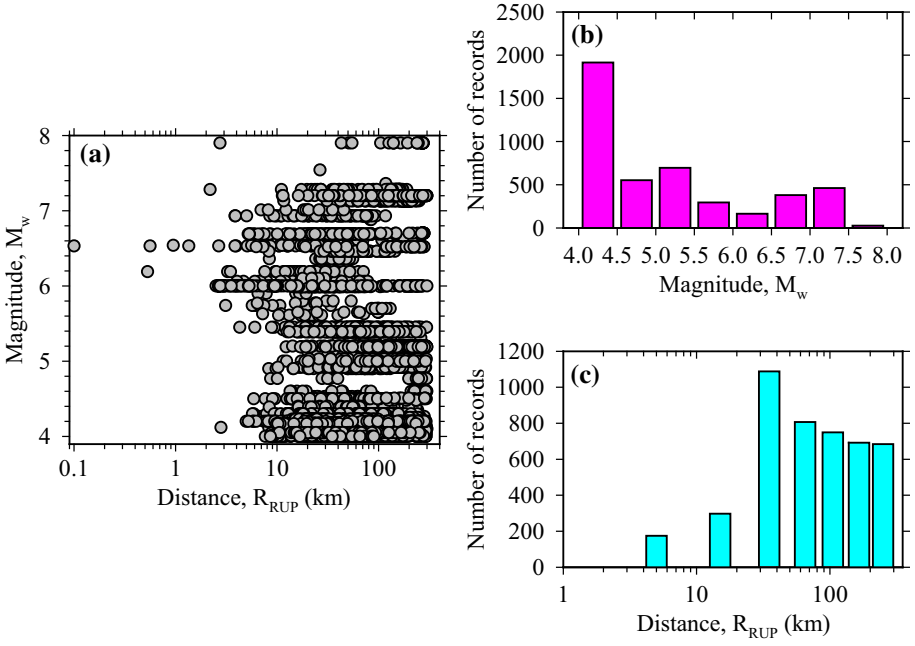

Fig. 3 The distribution of ground motion data: **a** R_{RUP} versus M_w scatter plots, **b** M_w histograms, and **c** R_{RUP} histograms

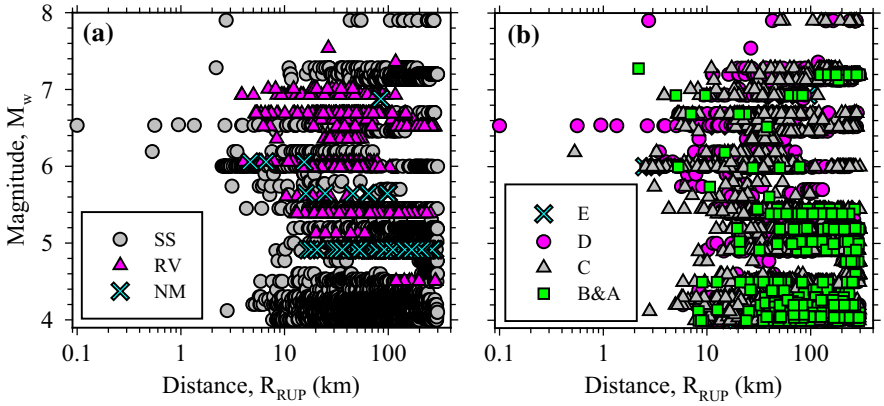

Fig. 4 Distribution of the recordings: **a** style-of-faulting and **b** NEHRP site classification

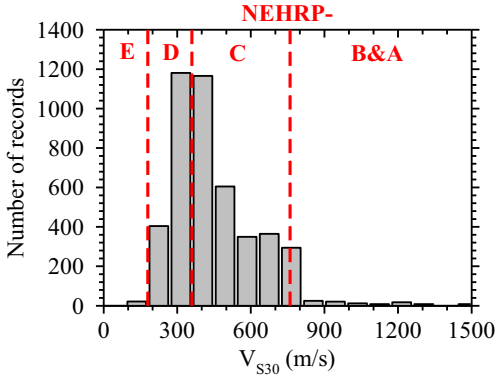

Fig. 5 V_{S30} histograms of the ground-motion database (*Note* One record has V_{S30} value beyond the upper range of the plot corresponding to NEHRP-A site class, $V_{S30} = 2016$ m/s)

4 Selection of the main functional form of the GMPE

The regression analysis to develop the PGR_α predictive model is conducted in multiple steps. To do so, the near-source database defined by R_{JB} and $R_{RUP} < 80$ km and the entire ground motion database (i.e. R_{JB} and $R_{RUP} < 300$ km) are utilized. As mentioned in the previous section, a distance of 80 km has been suggested as the approximate limit of interest for considering the significant effects of ground excitations on structural components (Campbell and Bozorgnia 2014). By using the near-source database limited at this distance, the fictitious depth term is computed and the terms of the model for the style-of-faulting are derived. Next, the rest of the regression coefficients such as magnitude scaling, hanging wall, site effects, etc. are obtained except for the constant term, magnitude-independent distance scaling and anelastic attenuation terms. To prevent jagged variations of spectral estimates, a limited amount of smoothing is applied to the regression coefficients. The rest of coefficients are computed by utilizing the entire ground motion database. Components of the aleatory variability model are obtained in a separate step using the

entire ground motion database. The final set of coefficients and standard deviation terms are derived using the random effects regression algorithm proposed by Abrahamson and Youngs (1992).

A simple statistical study is performed to determine the most suitable functional form for the PGR_α predictive model. An important point in selecting the functional form to develop a new GMPE is the ability of the model to take into account some crucial effects such as magnitude scaling, magnitude-dependent geometrical spreading, etc. (Bommer et al. 2010). Existing well-structured functional forms already include these key effects in their mathematical expressions. A number of candidate functional forms are considered in this study for their potential to predict PGR_α including those utilized by Abrahamson et al. (2014), ASK14; Boore et al. (2014), BSSA14; and Campbell and Bozorgnia (2014), CB14. These functional forms are evaluated only for modeling the magnitude scaling (f_{mag}), distance scaling (f_{dis}), style-of-faulting (f_{flt}), anelastic attenuation (f_{atn}) and linear site (f_{site}) effects in the GMPEs, in order to prevent complexity in preliminary assessments. In addition, a homoscedastic aleatory variability model is considered for the preliminary GMPEs.

Equations 3, 9 and 12 present the simplified functional forms of ASK14, BSSA14 and CB14, respectively which are referred to as basic form GMPEs. Magnitude scaling, distance scaling and style-of-faulting effect components of ASK14 and BSSA14 functions are given in Eqs. (4)–(8), 10, 11, respectively. The corresponding components for CB14 form are explained in detail in the next section (Median predictive model). The same linear site model given in Eq. (13) is considered for all functional forms.

$$\ln Y_{ASK14} = f_{mag} + f_{dis} + f_{flt} + f_{site} \tag{3}$$

$$f_{mag} = \begin{cases} a_1 + a_5(M_w - 6.75) + a_8(8.5 - M_w)^2; & M_w > 6.75 \\ a_1 + a_4(M_w - 6.75) + a_8(8.5 - M_w)^2; & 5.0 < M_w < 6.75 \\ a_1 + a_4(5.0 - 6.75) + a_8(8.5 - 5.0)^2 + a_6(M_w - 5.0) & \\ \quad + a_4(M_w - 6.75) + a_7(M_w - 5.0)^2; & M_w < 5.0 \end{cases} . \tag{4}$$

$$f_{dis} = \begin{cases} [a_2 + a_3(M_w - 6.75)] \ln\left(\sqrt{R_{RUP}^2 + h^2}\right) + a_{17} R_{RUP}; & M_w > 5.0 \\ [a_2 + a_3(5.0 - 6.75)] \ln\left(\sqrt{R_{RUP}^2 + h^2}\right) + a_{17} R_{RUP}; & M_w \le 5.0 \end{cases} \tag{5}$$

$$f_{flt} = f_{flt,F}\, f_{flt,M} \tag{6}$$

$$f_{flt,F} = a_8 F_{RV} + a_9 F_{NM} \tag{7}$$

$$f_{flt,M} = \begin{cases} 0; & M_w \le 4.5 \\ M_w - 4.5; & 4.5 < M_w \le 5.5 \\ 1; & M_w > 5.5 \end{cases} \tag{8}$$

where F_{NM} and F_{RV} are dummy variables equal to unity for normal (NM) and reverse faults (RV), respectively. For strike-slip (SS) events, F_{NM} and F_{RV} are zero.

$$\ln Y_{BSSA14} = f_{mag\&flt} + f_{dis} + f_{site} \tag{9}$$

$$f_{mag\&flt} = \begin{cases} a_1 SS + a_2 NS + a_3 RV + a_4(M_w - 5.5) + a_5(M_w - 5.5)^2; & M_w \le 5.5 \\ a_1 SS + a_2 NS + a_3 RV + a_6(M_w - 5.5); & M_w \le 5.5 \end{cases} \tag{10}$$

$$f_{dis} = [a_7 + a_8(M_w - 4.5)] \ln\left(\sqrt{R_{JB}^2 + a_7^2}\right) + a_9\left(\sqrt{R_{JB}^2 + a_7^2} - 1\right) \quad (11)$$

$$\ln Y_{CB14} = f_{mag} + f_{dis} + f_{flt} + f_{atn} + f_{site} \quad (12)$$

$$f_{site} = s_1 \min\left\{\ln\left(V_{S30}/1130\right), 0\right\} \quad (13)$$

Although the use of simplified functional forms may be considered as a cursory approach, the aim of this evaluation is to decrease the level of subjectivity by invoking statistical tools to select the functional form among the host of alternatives. The preliminary GMPEs are developed for peak ground fractional order IMs for the horizontal component of ground motions at $\alpha = 0$ (PGA), -0.25, -0.50, -0.75 and -1 (PGV). These IMs are computed using the average horizontal component definition referred to as RotD50 (Boore 2010). Figure 6 shows the magnitude scaling comparison between the candidate functional form GMPEs of this study and the NGA-West2 predictive models of ASK14, BSSA14, CB14 and CY14 (Chiou and Youngs 2014) at $\alpha = 0$ (PGA) and -1 (PGV) for an earthquake scenario with strike-slip faulting, $R_{RUP} = 10$ km and rock site condition ($V_{S30} = 760$ m/s). Results indicate that ground motion estimates from the basic form GMPEs are comparable with the spectral ordinates of the NGA-West2 predictive models. This agreement enhances confidence in the statistical tests conducted to select the main functional form of the GMPE.

A number of ground motion data-driven testing tools are considered for the evaluation of GMPEs; the tools include Nash and Sutcliffe Efficiency Coefficient (NSE; Nash and Sutcliffe 1970), Likelihood (LH; Scherbaum et al. 2004), Log-likelihood (LLH; Scherbaum et al. 2009) and Euclidean Distance Based Ranking (EDR; Kale and Akkar 2013; Akkar and Kale 2014). These tools are commonly used in testing the appropriateness of candidate predictive models for site specific or regional seismic hazard applications; however, they also provide ranking of GMPEs under a ground motion database. In addition, Akaike's and Bayesian Information Criterion (AIC and BIC, respectively) are also considered to rank the candidate functional forms. In this study, the NSE, LH, LLH and EDR ranking indices, and AIC and BIC statistical values are computed for the basic form GMPEs under the compiled ground motion database for $\alpha = 0$ (PGA), -0.25, -0.50,

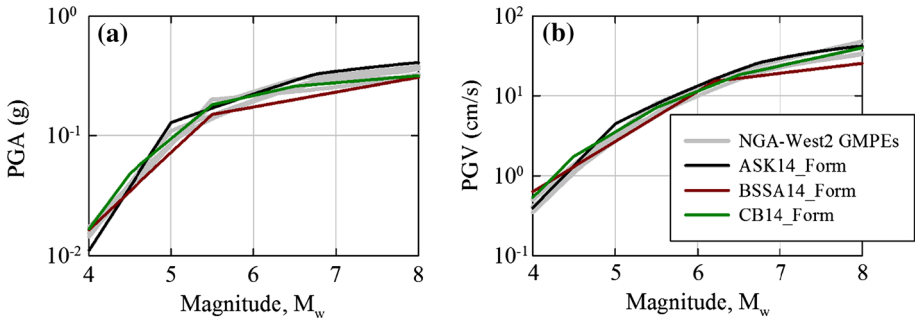

Fig. 6 Magnitude scaling comparison between the basic models and NGA-West2 GMPEs. The GMPE is evaluated for strike-slip faulting, $R_{RUP} = 10$ km, $V_{S30} = 760$ m/s, and dip = 90°. Default values of depth to shear wave velocity of 1.0 km/s ($Z_{1.0}$) and 2.5 km/s ($Z_{2.5}$) at the site, depth to top of rupture, hypocentral depth and rupture width are calculated from Kaklamanos et al. (2011). The R_{JB} values corresponding to $R_{RUP} = 10$ km are calculated from the virtual fault plane

Table 1 Average data-driven testing scores of the GMPEs with selected functional forms

Functional form	EDR	NSE	LH	LLH	AIC	BIC
ASK14	0.954	0.896	*0.50*	1.662	23.7	107.0
BSSA14	0.929	0.899	0.51	1.637	*19.7*	*90.2*
CB14	*0.913*	*0.902*	*0.50*	*1.620*	21.8	98.7

-0.75 and -1 (PGV). Table 1 lists the average scores of ranking indices that represent the overall performances of the basic form GMPEs for the considered α range. Among these indices, higher values of NSE, lower values of LLH, EDR, AIC and BIC, and values of LH around 0.5 indicate the best performance of GMPEs (or functional forms) under the considered ground motion database. The best performance of a predictive model could be interpreted as the effectiveness of the selected functional form to describe the characteristic features of the subject ground motion database. The underlined italic values in Table 1 indicate the best performing model (or models) for the implemented statistical methods. The basic functional form of CB14 shows the best performance among all data-driven testing tools and gives comparable criterion values among the statistical tools and thus this functional form is selected to develop the PGR_{α} predictive model.

5 Median predictive model

The final functional form of the PGR_{α} predictive model accounts for magnitude, distance, style-of-faulting, linear and nonlinear site, hanging wall, basin response, and anelastic distance attenuation effects. Equation 14 shows the complete functional form for estimating the average horizontal component (RotD50; Boore 2010) median peak ground fractional responses ($cm/s^{2+\alpha}$) at 21 α values ranging from 0 (PGA) to -1 (PGV) in natural logarithm unit. Fractional orders less than -1 are not considered because the low frequency content of accelerograms starts to become important in the range of PGD, which is highly sensitive to the low-cut filtering process of ground motion recordings. Each component of final functional form in Eq. (14) is briefly explained in the following paragraphs.

$$\ln Y = f_{mag} + f_{dis} + f_{flt} + f_{hng} + f_{sed} + f_{atn} + f_{site} \tag{14}$$

The magnitude scaling model includes three breaks at moment magnitudes M_w 4.5, 5.5 and 6.5 to characterize the ground motions as follows:

$$f_{mag} = \begin{cases} a_0 + a_1 M_w; & M_w \le 4.5 \\ a_0 + a_1 M_w + a_2(M_w - 4.5); & 4.5 < M_w \le 5.5 \\ a_0 + a_1 M_w + a_2(M_w - 4.5) + a_3(M_w - 5.5); & 5.5 < M_w \le 6.5 \\ a_0 + a_1 M_w + a_2(M_w - 4.5) + a_3(M_w - 5.5) + a_4(M_w - 6.5); & M_w > 6.5 \end{cases} \tag{15}$$

The distance scaling (geometrical spreading) model is presented in Eq. (16). This model implements the R_{RUP} distance metric as the main distance measure.

$$f_{dis} = (a_5 + a_6 M_w) \ln\left(\sqrt{R_{RUP}^2 + a_7^2}\right) \tag{16}$$

where a_7 coefficient is the fictitious depth term. The style-of-faulting model given in Eqs. (17)–(19) is magnitude dependent. F_{NM} and F_{RV} are dummy variables equal to unity for normal (NM) and reverse faults (RV), respectively. For strike-slip (SS) events, F_{NM} and F_{RV} are zero. No correction is suggested for reverse events as no difference is observed in the spectral trends between SS and RV ground motion data in the database.

$$f_{flt} = f_{flt,F}\, f_{flt,M} \tag{17}$$

$$f_{flt,F} = a_8 F_{RV} + a_9 F_{NM} \tag{18}$$

$$f_{flt,M} = \begin{cases} 0; & M_w \leq 4.5 \\ M_w - 4.5; & 4.5 < M_w \leq 5.5 \\ 1; & M_w > 5.5 \end{cases} \tag{19}$$

The hanging wall model of Donahue and Abrahamson (2014) with some modifications by Abrahamson et al. (2014) is employed in the predictive model as shown in Eq. (20). Some of the model coefficients of Donahue and Abrahamson (2014) are period dependent. The modifications performed by Abrahamson et al. (2014) on the original model of Donahue and Abrahamson (2014) provide period-independent hanging wall model coefficients (except for a_{10} coefficient), rendering the implementation of this model for the PGR_α GMPE feasible. The hanging wall model considers the effects of dip angle (Eq. 21), M_w (Eq. 22 where magnitude scaling hanging wall term, $a_{HW} = 0.2$), R_X (closest distance to the surface projection of the top edge of fault rupture, Eqs. (23)–(25) where $h_1 = 0.25$, $h_2 = 1.5$ and $h_3 = -0.75$, and W is the fault rupture width), Z_{TOR} (depth to top of fault rupture, Eq. 26), and R_{JB} (Joyner-Boore distance, Eq. 27) for sites located on hanging wall side of the fault rupture (i.e. $F_{HW} = 1$). For other site locations (i.e. $F_{HW} = 0$), hanging wall effects are not considered in the ground motion estimates.

$$f_{hng} = a_{10} F_{HW}\, f_{hng,dip}\, f_{hng,M_w}\, f_{hng,R_X}\, f_{hng,Z_{TOR}}\, f_{hng,R_{JB}} \tag{20}$$

$$f_{hng,dip} = \begin{cases} (90 - dip)/45; & dip > 30 \\ 60/45; & dip \leq 30 \end{cases} \tag{21}$$

$$f_{hng,M_w} = \begin{cases} 1 + a_{HW}(M_w - 6.5); & M_w \geq 6.5 \\ 1 + a_{HW}(M_w - 6.5) - (1 - a_{HW})(M_w - 6.5)^2; & 5.5 < M_w < 6.5 \\ 0; & M_w \leq 5.5 \end{cases} \tag{22}$$

$$f_{hng,R_X} = \begin{cases} h_1 + h_2\left(R_X/R_1\right) + h_3\left(R_X/R_1\right)^2; & R_X < R_1 \\ 1 - \left(\dfrac{R_X - R_1}{R_2 - R_1}\right); & R_1 \leq R_X \leq R_2 \\ 0; & R_X > R_2 \end{cases} \tag{23}$$

$$R_1 = W\cos(dip) \tag{24}$$

$$R_2 = 3R_1 \tag{25}$$

$$f_{hng,Z_{TOR}} = \begin{cases} 1 - \dfrac{Z_{TOR}^2}{100}; & Z_{TOR} \leq 10 \\ 0; & Z_{TOR} > 10 \end{cases} \tag{26}$$

$$f_{hng,R_{JB}} = \begin{cases} 1; & R_{JB} = 0 \\ 1 - R_{JB}/30; & R_{JB} < 30 \\ 0; & R_{JB} \geq 30 \end{cases} \quad (27)$$

The basin response model is given in Eq. (28) which is based on the depth to the 2.5 km/s shear wave velocity horizon beneath the site ($Z_{2.5}$). The k coefficient in this equation is equal to 1.88. In case $Z_{2.5}$ parameter is not available, its value can be inferred from the simple empirical relationship proposed by Campbell and Bozorgnia (2014) for Californian sites as given in Eq. (29).

$$f_{sed} = \begin{cases} a_{11}(Z_{2.5} - 1); & Z_{2.5} \leq 1 \\ 0; & 1 < Z_{2.5} \leq 3 \\ a_{12}\, k\, e^{-0.75}\left(1 - e^{-0.25(Z_{2.5}-1)}\right); & Z_{2.5} > 3 \end{cases} \quad (28)$$

$$Z_{2.5} = \exp(7.089 - 1.144 \ln(V_{S30})) \quad (29)$$

The anelastic attenuation model is given in Eq. (30) which reflects attenuation effects in the ground motion estimates for sites with $R_{RUP} > 80$ km.

$$f_{atn} = \begin{cases} a_{13}(R_{RUP} - 80); & R_{RUP} > 80 \\ 0; & R_{RUP} \leq 80 \end{cases} \quad (30)$$

The site response model is given in Eq. (31) which is adapted from Chiou and Youngs (2014) primarily due to its simplicity. In this equation, f_{lin} and f_{nl} represent the linear and nonlinear components of site amplification, respectively. The linear site effects are taken into account using Eq. (32) where s_1 describes the V_{S30} scaling whereas $V_{S30} = 1130$ m/s is the reference site condition beyond which the site amplification is not considered. The nonlinear site function is given in Eq. (33) where s_2 represents the degree of nonlinearity as a function of V_{S30} and can be obtained from Eq. (34). In Eq. (33), PGR_{1130} is the median peak ground fractional response computed from Eq. (14) for the reference rock site condition (i.e. $V_{S30} = 1130$ m/s).

$$f_{site} = f_{lin} + f_{nl} \quad (31)$$

$$f_{lin} = s_1 \min\left\{\ln\left(V_{S30}/1130\right), 0\right\} \quad (32)$$

$$f_{nl} = s_2 \ln\left(\frac{PGR_{1130} + s_3}{s_3}\right) \quad (33)$$

$$s_2 = s_4\left[e^{s_5(\min(V_{S30},1130)-360)} - e^{s_5(1130-360)}\right] \quad (34)$$

One considered strategy for determining site response model coefficients would be to directly adopt Chiou and Youngs (2014) nonlinear model coefficients (s_3, s_4 and s_5) while obtaining the linear site model coefficient (s_1) from the regression analysis to reflect the site effects of the chosen ground motion database in the functional form. However this process is not feasible since nonlinear site model coefficients are not available for fractional orders except for $\alpha = 0$ (i.e. PGA) and $\alpha = -1$ (i.e. PGV). As an alternative, a separate regression analysis is performed to derive the site coefficients for intermediate fractional orders (i.e. $\alpha = -0.05$ to -0.95) by implementing the basic functional form GMPE as in Sect. 4 (i.e. Selection of the main functional form of the GMPE). The

Table 2 α-independent constant regression coefficients

a_7	a_8	a_9
4.5	0.0	−0.1

Table 3 α-dependent magnitude and distance scaling model regression coefficients

α	a_0	a_1	a_2	a_3	a_4	a_5	a_6
0 (PGA)	1.150	1.407	−0.827	−0.956	−0.223	−2.964	0.307
−0.05	0.905	1.416	−0.832	−0.939	−0.234	−2.952	0.306
−0.1	0.645	1.428	−0.836	−0.919	−0.246	−2.935	0.304
−0.15	0.402	1.437	−0.839	−0.899	−0.257	−2.924	0.303
−0.2	0.168	1.446	−0.844	−0.881	−0.269	−2.908	0.301
−0.25	−0.074	1.457	−0.849	−0.862	−0.281	−2.893	0.299
−0.3	−0.310	1.467	−0.855	−0.840	−0.292	−2.882	0.298
−0.35	−0.593	1.486	−0.862	−0.815	−0.304	−2.866	0.296
−0.4	−0.871	1.506	−0.870	−0.796	−0.315	−2.845	0.293
−0.45	−1.129	1.523	−0.878	−0.780	−0.327	−2.825	0.290
−0.5	−1.394	1.542	−0.887	−0.764	−0.339	−2.806	0.287
−0.55	−1.671	1.563	−0.897	−0.740	−0.350	−2.791	0.285
−0.6	−1.947	1.584	−0.907	−0.714	−0.362	−2.770	0.282
−0.65	−2.226	1.606	−0.917	−0.683	−0.374	−2.755	0.280
−0.7	−2.525	1.632	−0.928	−0.647	−0.385	−2.729	0.276
−0.75	−2.844	1.662	−0.939	−0.609	−0.397	−2.703	0.272
−0.8	−3.135	1.688	−0.951	−0.573	−0.408	−2.683	0.269
−0.85	−3.422	1.714	−0.962	−0.535	−0.420	−2.658	0.265
−0.9	−3.691	1.737	−0.974	−0.497	−0.432	−2.642	0.263
−0.95	−3.936	1.756	−0.985	−0.467	−0.443	−2.627	0.261
−1 (PGV)	−4.167	1.772	−0.997	−0.442	−0.455	−2.610	0.259

regression analysis is constrained to derive the same nonlinear coefficients (i.e. s_3, s_4 and s_5) as those given in Chiou and Youngs (2014) for PGA and PGV, therefore compatible coefficients for the intermediate fractional orders are derived. Then these nonlinear site coefficients are directly used in the site response model of the final predictive model. The values of s_1 for the linear site model coefficient are derived again in the final regressions to consider the effects of the complete functional form.

The full set of α-independent and -dependent regression coefficients for the median PGR_α predictive model is provided in Tables 2, 3 and 4.

6 Aleatory variability model

The total aleatory variability (σ) can be partitioned into the between-event (τ, M_w-dependent) and within-event (ϕ, M_w- and V_{S30}-dependent) standard deviation terms as given in Eq. (35).

Table 4 α-dependent hanging wall, basin response, anelastic attenuation and site response model regression coefficients

α	a_{10}	a_{11}	a_{12}	a_{13}	s_1	s_3	s_4	s_5
0 (PGA)	0.482	−0.056	0.371	−0.0071	−0.396	100.00	−0.1417	−0.00701
−0.05	0.477	−0.043	0.378	−0.0069	−0.406	89.74	−0.1419	−0.00713
−0.1	0.478	−0.030	0.385	−0.0067	−0.417	79.35	−0.1418	−0.00725
−0.15	0.480	−0.017	0.393	−0.0064	−0.430	68.81	−0.1412	−0.00737
−0.2	0.487	−0.005	0.400	−0.0062	−0.441	60.68	−0.1403	−0.00747
−0.25	0.502	0.008	0.404	−0.0060	−0.453	53.37	−0.1389	−0.00757
−0.3	0.524	0.021	0.410	−0.0057	−0.464	47.02	−0.1371	−0.00767
−0.35	0.547	0.033	0.417	−0.0055	−0.475	41.41	−0.1349	−0.00776
−0.4	0.565	0.045	0.423	−0.0053	−0.486	36.25	−0.1323	−0.00785
−0.45	0.581	0.055	0.433	−0.0050	−0.496	31.81	−0.1294	−0.00793
−0.5	0.598	0.064	0.444	−0.0048	−0.507	27.91	−0.1260	−0.00800
−0.55	0.618	0.074	0.456	−0.0045	−0.517	24.32	−0.1222	−0.00807
−0.6	0.632	0.085	0.463	−0.0043	−0.528	21.21	−0.1180	−0.00813
−0.65	0.642	0.097	0.472	−0.0041	−0.538	18.22	−0.1134	−0.00819
−0.7	0.647	0.109	0.483	−0.0038	−0.550	15.40	−0.1084	−0.00824
−0.75	0.652	0.122	0.497	−0.0036	−0.561	13.12	−0.1030	−0.00829
−0.8	0.651	0.135	0.512	−0.0034	−0.572	11.04	−0.0972	−0.00833
−0.85	0.653	0.148	0.527	−0.0032	−0.582	9.11	−0.0910	−0.00837
−0.9	0.654	0.162	0.539	−0.0030	−0.589	7.69	−0.0843	−0.00840
−0.95	0.659	0.175	0.547	−0.0028	−0.596	6.47	−0.0773	−0.00842
−1 (PGV)	0.665	0.188	0.552	−0.0026	−0.602	5.41	−0.0699	−0.00844

$$\sigma(M_w, V_{S30}) = \sqrt{\tau^2(M_w) + \phi^2(M_w, V_{S30})} \tag{35}$$

The M_w-dependent between-event standard deviation term is modeled by:

$$\tau(M_w) = \begin{cases} \tau_1; & M_w \leq 4.5 \\ \tau_1 + (\tau_2 - \tau_1)(M_w - 4.5); & 4.5 < M_w < 5.5 \\ \tau_2; & M_w \geq 5.5 \end{cases} \tag{36}$$

The M_w- and V_{S30}-dependent within-event standard deviation term is modeled by:

$$\phi(M_w, V_{S30}) = \begin{cases} \phi(M_w); & V_{S30} \geq V_2 \\ \phi(M_w) - \Delta\phi_V \left(\dfrac{\ln(V_2/V_{S30})}{\ln(V_2/V_1)} \right); & V_1 < V_{S30} < V_2 \\ \phi(M_w) - \Delta\phi_V; & V_{S30} \leq V_1 \end{cases} \tag{37}$$

where $V_1 = 225$ m/s and $V_2 = 300$ m/s are selected from the residual trends and $\phi(M_w)$ is computed by:

$$\phi(M_w) = \begin{cases} \phi_1; & M_w \leq 4.5 \\ \phi_1 + (\phi_2 - \phi_1)(M_w - 4.5); & 4.5 < M_w < 5.5 \\ \phi_2; & M_w \geq 5.5 \end{cases} \tag{38}$$

The aleatory variability model is developed by evaluating the M_w bins of between-event residuals (η_i) to obtain between-event standard deviations τ, and the M_w, R_{RUP} and V_{S30} bins of within-event residuals (ε_{ij}) to obtain within-event standard deviations ϕ. The τ and ϕ values are computed corresponding to the generated bins from the random effects regression algorithm (Abrahamson and Youngs 1992). Figures 7 and 8 display the aleatory

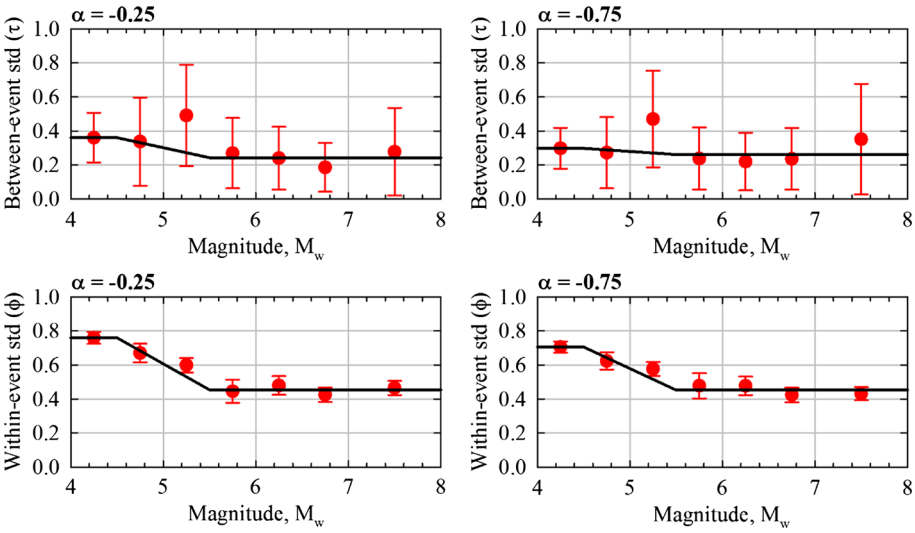

Fig. 7 Binned aleatory variability terms and their 95% confidence intervals for fractional order, $\alpha = -0.25$ (*left column*) and -0.75 (*right column*), and between-event standard deviation, τ, (*upper row*) and within-event standard deviation, ϕ, (*bottom row*) against M_w

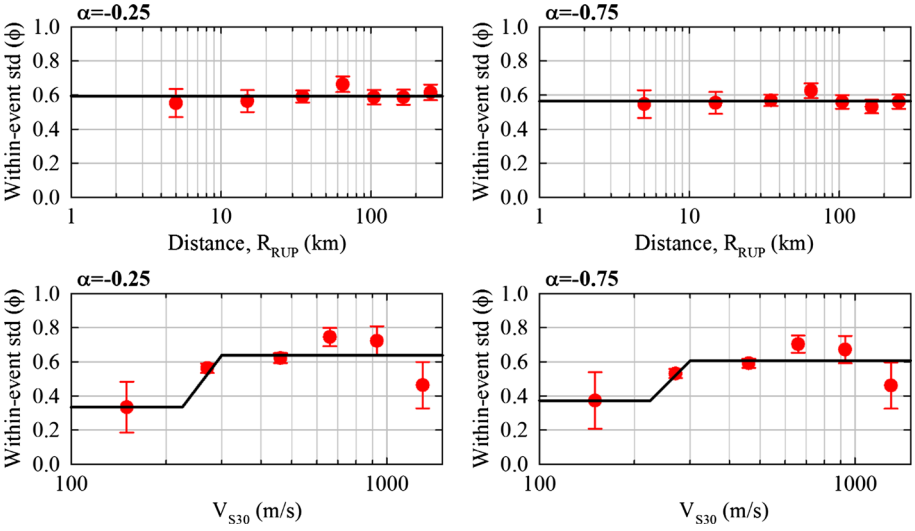

Fig. 8 Binned aleatory variability terms and their 95% confidence intervals for fractional order, $\alpha = -0.25$ (*left column*) and -0.75 (*right column*), and within-event standard deviation, ϕ, against R_{RUP} (*upper row*) and within-event standard deviation, ϕ, against V_{S30} (*bottom row*)

variability terms calculated for these bins as well as their 95% confidence intervals and final aleatory variability model fits (solid linear or trilinear functions) for the representative fractional orders. Figure 7 shows the magnitude-dependent main τ and ϕ models. Two breaks are selected at $M_w = 4.5$ and 5.5 from the general trends of the binned aleatory variability terms. In Eqs. (36) and (38), $\tau_1-\phi_1$ and $\tau_2-\phi_2$ pairs represent the aleatory variability terms for $M_w \leq 4.5$ and $M_w \geq 5.5$, respectively. Path and site effects on the within-event aleatory variability term are investigated from Fig. 8. The binned ϕ trends in the upper row of Fig. 8 show no dependence of ϕ upon R_{RUP} for path effects whereas the binned ϕ trends in the bottom row of this figure indicate that the final within-event standard deviation term should account for site effects given observed dependence of ϕ upon V_{S30}.

The binned ϕ trends (bottom row of Fig. 8) indicate that ϕ is constant for small values of V_{S30}, increases afterwards with V_{S30} up to a certain value and then follows an almost stable trend. Two breaks are selected at $V_{S30} = 225$ m/s and 300 m/s to fit a suitable model to within-event standard deviations by evaluating the V_{S30} versus ε_{ij} residual trends in conjunction with the V_{S30} versus ϕ behaviors. These selections also comply with the observations of Boore et al. (2014). Thus a reduction to ϕ values calculated from Eq. (38) is proposed for sites with $V_{S30} < V_2 = 300$ m/s. The application of this reduction is proposed by the introduction of a $\Delta\phi_v$ parameter in Eq. (37) which has a similar form as the equation in Boore et al. (2014) predictive model. To obtain a generic $\Delta\phi_v$ parameter, the within-event standard deviation terms are computed for $M_w \leq 4.5$ (i.e. ϕ_1) and $M_w \geq 5.5$ (i.e. ϕ_2) separately corresponding to ε_{ij} for no V_{S30} limitation (i.e. complete residuals), ε_{ij} for $V_{S30} < 225$ m/s and ε_{ij} for $V_{S30} > 300$ m/s. The upper row of Fig. 9 shows the variations of the corresponding ϕ_1 and ϕ_2 values with respect to the fractional order. The calculated ϕ_1 and ϕ_2 values of the complete residuals and the residuals for $V_{S30} > 300$ m/s almost overlap each other whereas ϕ_1 and ϕ_2 values of the residuals for $V_{S30} < 225$ m/s differ from the complete standard deviations. The differences in ϕ values for the latter case (i.e. $V_{S30} < 225$ m/s) are calculated and the variations for $M_w \leq 4.5$ (i.e.

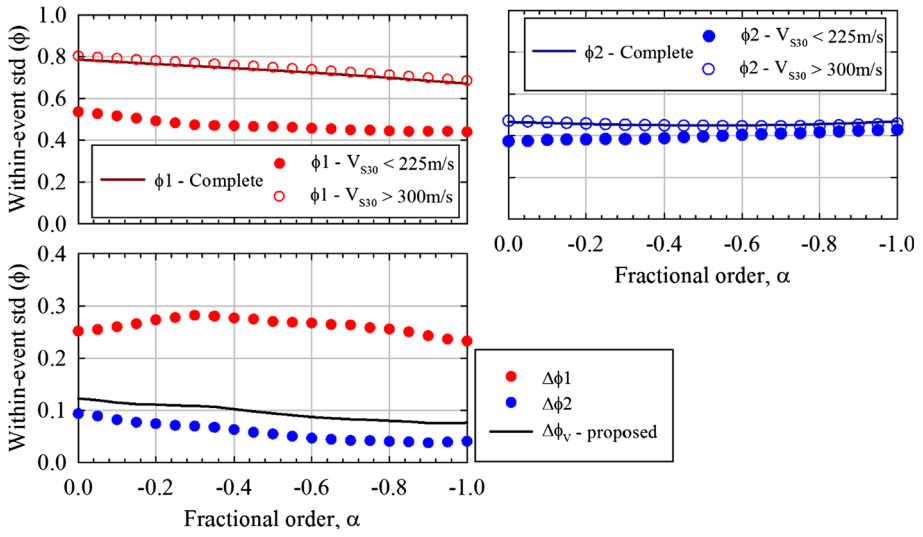

Fig. 9 Effects of V_{S30} on within-event standard deviation terms (*upper row*) and the proposed reduction parameter ($\Delta\phi_v$) for ground motion data with $V_{S30} \leq 300$ m/s (*bottom row*)

Table 5 α-dependent standard deviations and reduction parameter

α	τ_1	τ_2	ϕ_1	ϕ_2	$\Delta\phi_v$
0 (PGA)	0.391	0.239	0.786	0.466	0.123
−0.05	0.385	0.240	0.781	0.463	0.119
−0.1	0.380	0.241	0.775	0.461	0.115
−0.15	0.373	0.243	0.770	0.458	0.112
−0.2	0.368	0.243	0.765	0.456	0.111
−0.25	0.360	0.243	0.760	0.454	0.109
−0.3	0.353	0.245	0.755	0.452	0.109
−0.35	0.348	0.246	0.750	0.451	0.107
−0.4	0.343	0.247	0.745	0.450	0.102
−0.45	0.336	0.249	0.740	0.450	0.098
−0.5	0.329	0.250	0.735	0.450	0.094
−0.55	0.321	0.252	0.729	0.449	0.091
−0.6	0.316	0.256	0.724	0.450	0.087
−0.65	0.311	0.258	0.718	0.450	0.085
−0.7	0.303	0.260	0.712	0.451	0.083
−0.75	0.298	0.261	0.705	0.453	0.082
−0.8	0.292	0.264	0.699	0.455	0.080
−0.85	0.287	0.266	0.692	0.458	0.078
−0.9	0.281	0.270	0.685	0.461	0.076
−0.95	0.276	0.275	0.678	0.465	0.076
−1 (PGV)	0.281	0.281	0.672	0.468	0.076

$\Delta\phi_1$) and $M_w \geq 5.5$ (i.e. $\Delta\phi_2$) are shown in the bottom row of Fig. 9. The variations in $\Delta\phi_1$ and $\Delta\phi_2$ suggest a considerable reduction in within-event standard deviation of small magnitude ground motion data whereas the reduction is modest for the ones of moderate-to-large magnitudes. To simplify the aleatory variability model, a magnitude-independent $\Delta\phi_v$ reduction parameter is proposed based on the weighted average of $\Delta\phi_1$ and $\Delta\phi_2$ based upon the number of ground motion data included in the bins of $M_w \leq 4.5$ and $M_w \geq 5.5$. The variation of the proposed reduction parameter $\Delta\phi_v$ with respect to fractional order is shown in Fig. 9. Fractional order dependent between-event and within-event standard deviations together with the reduction parameter are listed in Table 5.

7 Evaluation of the proposed GMPE

First, the residuals (i.e. the difference between median prediction and empirical data) of the predictive model computed from the random effect regression analysis are evaluated to scrutinize the deviation between ground motion estimates of the proposed GMPE and the empirical observations from the model development database. Figures 10, 11 and 12 display between-event (or inter-event) residuals (η_i) versus M_w, and within-event (or intra-event) residuals (ε_{ij}) versus R_{RUP} and V_{S30} for fractional orders, $\alpha = 0$ (PGA), −0.25, −0.50 and −1 (PGV). The between-event residuals for M_w and within-event residuals for R_{RUP} and V_{S30} do not indicate any systematic variations that point out biased estimates for the ground motion database. The corresponding mean binned residuals and their confidence limits also fluctuate about zero which implies unbiased ground motion estimates of

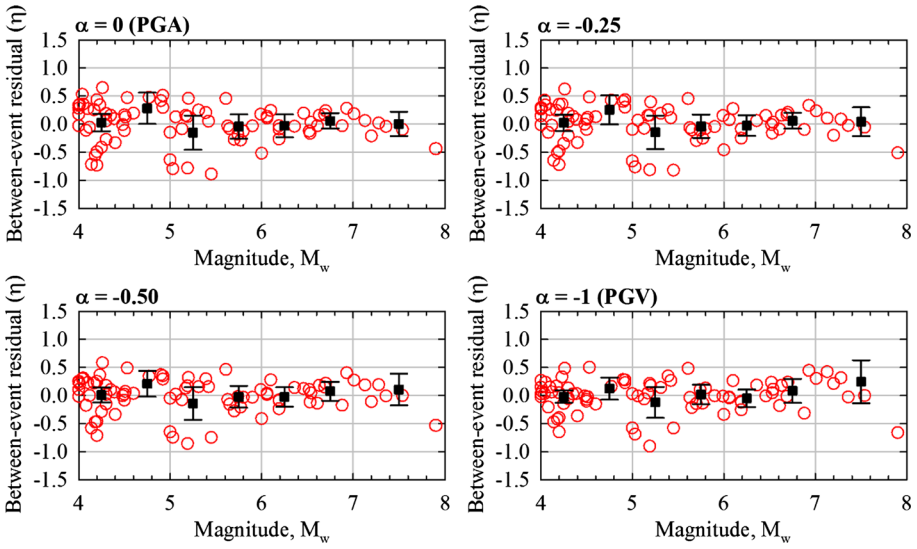

Fig. 10 Between-event residual (η_i) distribution against M_w of the predictive model for fractional orders, $\alpha = 0$, -0.25, -0.50 and -1. The *error bars* indicate 95% confidence intervals of the mean binned residuals

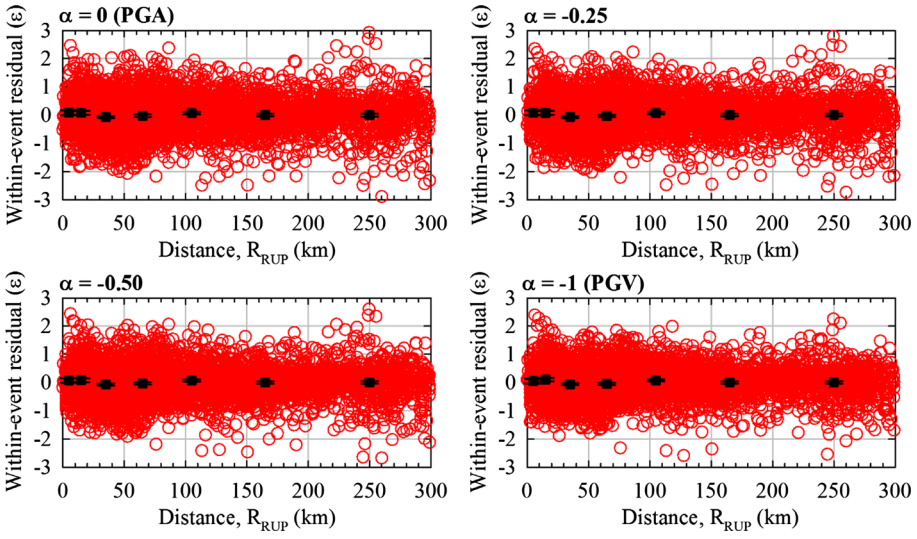

Fig. 11 Within-event residual (ε_{ij}) distribution against R_{RUP} of the predictive model for fractional orders, $\alpha = 0$, -0.25, -0.50 and -1. The *error bars* indicate 95% confidence intervals of the mean binned residuals

the proposed GMPE with respect to the main estimator parameters (i.e. M_w, R_{RUP} and V_{S30}).

A number of illustrative examples are provided to present scaling of the proposed GMPE with main estimator parameters (i.e. M_w, R_{RUP} and V_{S30}) and α values as well as

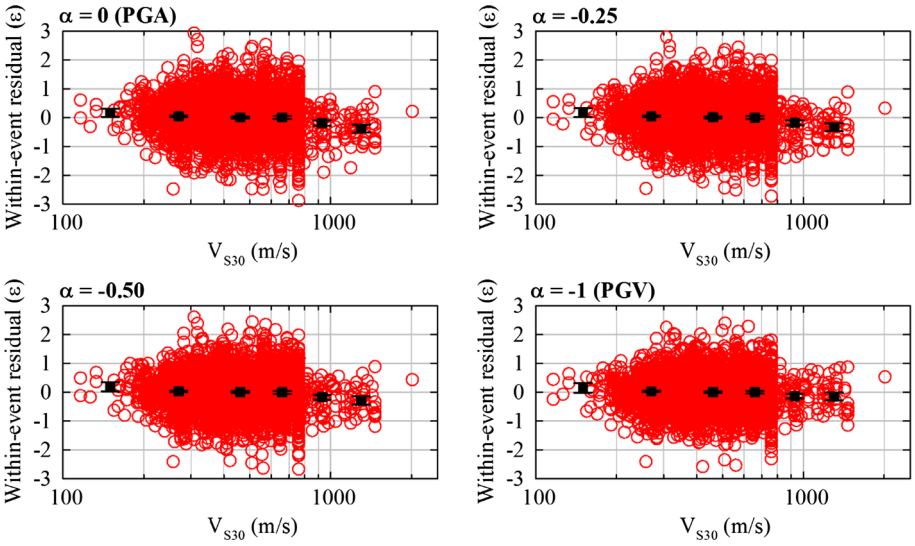

Fig. 12 Within-event residual (ε_{ij}) distribution against V_{S30} of the predictive model for fractional orders, $\alpha = 0$, -0.25, -0.50 and -1. The *error bars* indicate 95% confidence intervals of the mean binned residuals

comparisons with the ground motion estimates and aleatory variability components of the NGA-West2 predictive models. An earthquake scenario with vertical strike-slip fault mechanism is designated for all cases. To calculate the secondary estimator parameters (e.g. $Z_{1.0}$, $Z_{2.5}$, Z_{TOR}, Z_{HYP}, W, etc.), the relationships proposed in Kaklamanos et al. (2011) are utilized. The R_{JB} extended-source distances corresponding to the selected R_{RUP} metrics are calculated from the virtual fault planes considering the magnitude-dependent Z_{TOR} values.

Figures 13 and 14 compare the magnitude and distance scaling of the proposed predictive model with the NGA-West2 GMPEs. The comparisons are given at $R_{RUP} = 10$ km and 40 km for distance scaling, and $M_w = 5.5$ and 7.5 for magnitude scaling for a site condition with $V_{S30} = 760$ m/s. The comparisons are made for PGA and PGV which are the common IMs between the proposed model and the NGA-West2 GMPEs. In Fig. 14, the distance scaling curves start at the smallest possible R_{RUP} value, given its relation to the magnitude-dependent Z_{TOR} value which is deep for small magnitude earthquakes but shallow (even zero) for large magnitude events. The magnitude and distance scaling of the proposed GMPE show good agreement with the ground motion estimates of the NGA-West2 models for the selected earthquake scenarios. For small magnitude ranges ($M_w < 5$) in Fig. 13, ground motion estimates from the proposed model are slightly larger than estimates from the other models. The difference in the lower magnitude bounds of the proposed GMPE ($M_w = 4$) and the others ($M_w \sim 3$) may be one of the reasons for this observation. Bommer et al. (2007) highlighted that minimum magnitude (M_{min}) limits of databases would control the spectral estimates at small magnitudes; the predictive models that use a ground motion database with lower M_{min} may yield smaller ground motion estimates than those developed from a ground motion database with higher M_{min}. Overall, given that the PGR_α GMPE was developed to also consider the effect of α, the proposed predictive model offers a comparable estimate of integer order PGRs across M_w and R_{RUP}

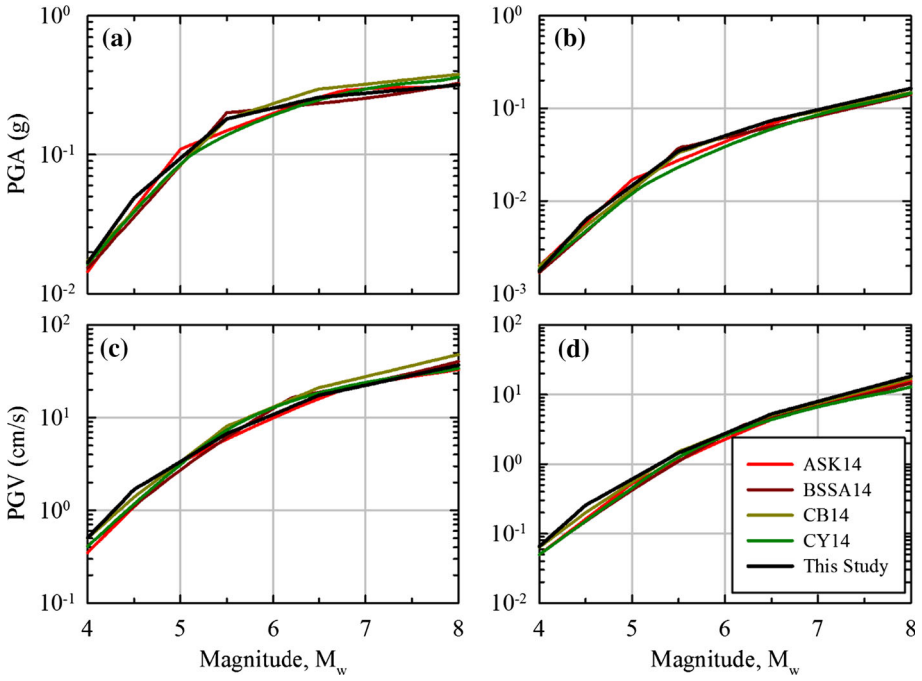

Fig. 13 Magnitude scaling comparison of the proposed GMPE with the NGA-West2 models for strike-slip events and $V_{S30} = 760$ m/s: **a** PGA, $R_{RUP} = 10$ km; **b** PGA, $R_{RUP} = 40$ km; **c** PGV, $R_{RUP} = 10$ km; **d** PGV, $R_{RUP} = 40$ km

to those proposed by NGA-West2 models while also enabling assessment of fractional order behavior.

Fractional order scaling of the proposed GMPE with magnitude for $V_{S30} = 760$ m/s and 255 m/s, and V_{S30} for $M_w = 4.5$ and 7.5 is represented in Figs. 15 and 16 at distance level of $R_{RUP} = 10$ km for strike-slip earthquakes. The magnitude effects for small-to-large magnitude levels of $M_w = 4.5$, 5.5, 6.5 and 7.5 are explored whereas the importance of V_{S30} is examined for soft-to-rock site conditions with $V_{S30} = 255$, 520, 760 and 1130 m/s. The plots of fractional order scaling with magnitude (Fig. 15) depict the fact that the decrease in the PGR_α values for small magnitudes ($M_w = 4.5$ and 5.5) is quadratic; however, this behavior changes gradually (turns into cubic) for both site classes as the magnitude increases. In addition, the large PGR_α differences between small magnitudes become narrower through moderate-to-large magnitudes due to magnitude saturation effects up to around $\alpha = -0.5$ (after that level, magnitude saturation effects are diminished; see Fig. 13c). While soil nonlinearity effects are not observed in fractional order scaling with V_{S30} plots for small magnitude events (Fig. 16a), those effects are detected in the evaluations of scaling for large magnitude (Fig. 16b) earthquakes for soft and stiff sites (i.e. $V_{S30} = 255$ and 520 m/s, respectively), and α values between 0 and -0.5.

Figure 17 presents the comparison of aleatory variability components (i.e. between-event, τ, and within-event, ϕ, standard deviations) of the proposed predictive model and selected NGA-West2 GMPEs for PGA and PGV levels as well as the τ and ϕ values of the proposed model at the intermediate α levels. The comparisons are made for two different magnitude and V_{S30} levels because of the M_w and V_{S30} dependency of the proposed

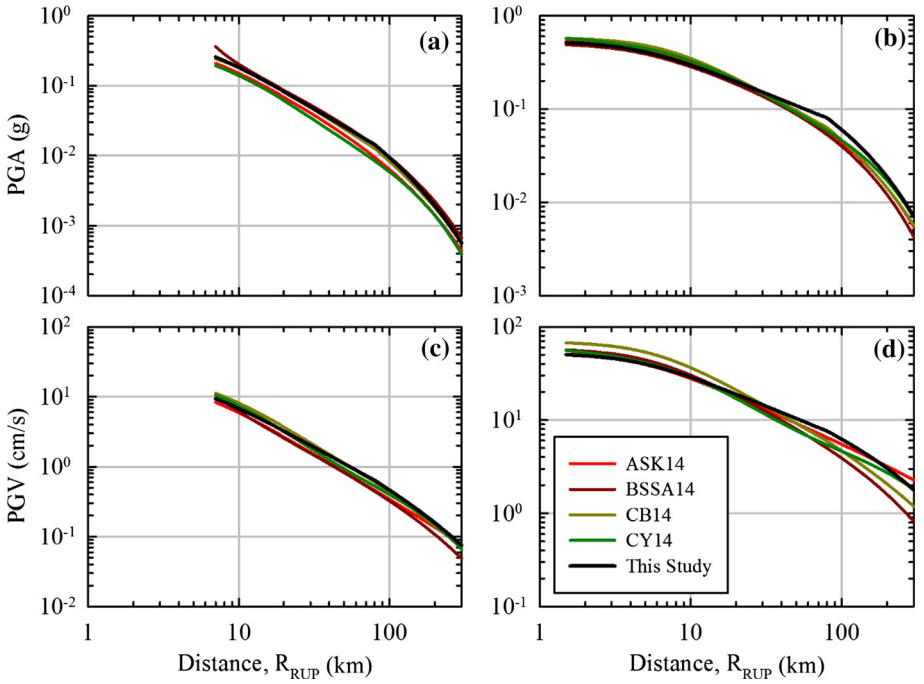

Fig. 14 Distance scaling comparison of the proposed GMPE with the NGA-West2 models for strike-slip events and $V_{S30} = 760$ m/s: **a** PGA, $M_w = 5.5$; **b** PGA, $M_w = 7.5$; **c** PGV, $M_w = 5.5$; **d** PGV, $M_w = 7.5$

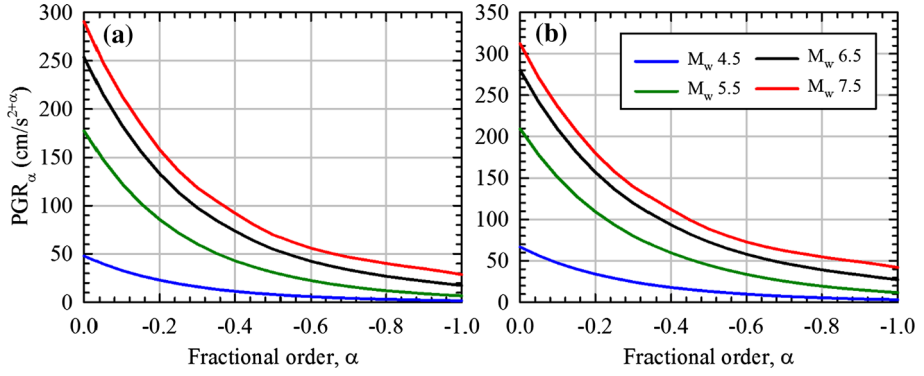

Fig. 15 Fractional order scaling with magnitude of the proposed predictive model for strike-slip earthquakes and $R_{RUP} = 10$ km: **a** $V_{S30} = 760$ m/s, **b** $V_{S30} = 255$ m/s

aleatory variability model (see Eqs. 35–38). Figure 17a shows a case for $M_w = 7.5$ and $V_{S30} = 760$ m/s whereas Fig. 17b displays a comparison for $M_w = 4.5$ and $V_{S30} = 255$ m/s. In general, the values of aleatory variability components of the proposed GMPE are within the corresponding bounds of the NGA-West2 models. The slight dissimilarities at PGA and PGV levels can be attributed to the differences of the size of the model development databases (NGA-West2 models have larger ground motion databases than the GMPE in this study) and lower magnitude bounds (NGA-West2 models have

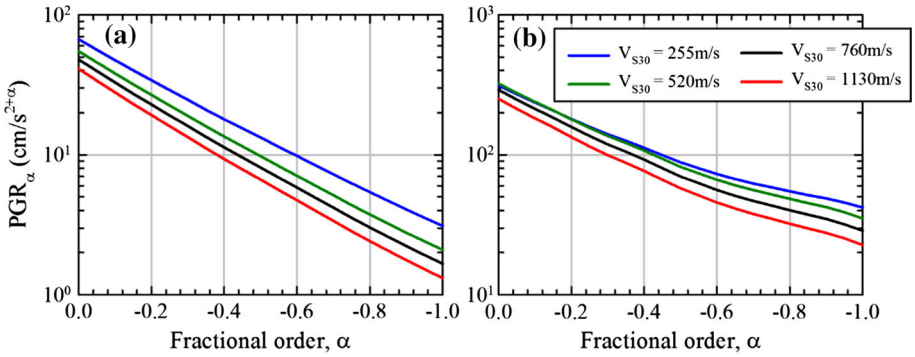

Fig. 16 Fractional order scaling with V_{S30} of the proposed predictive model for strike-slip earthquakes and $R_{RUP} = 10$ km: **a** $M_w = 4.5$, **b** $M_w = 7.5$

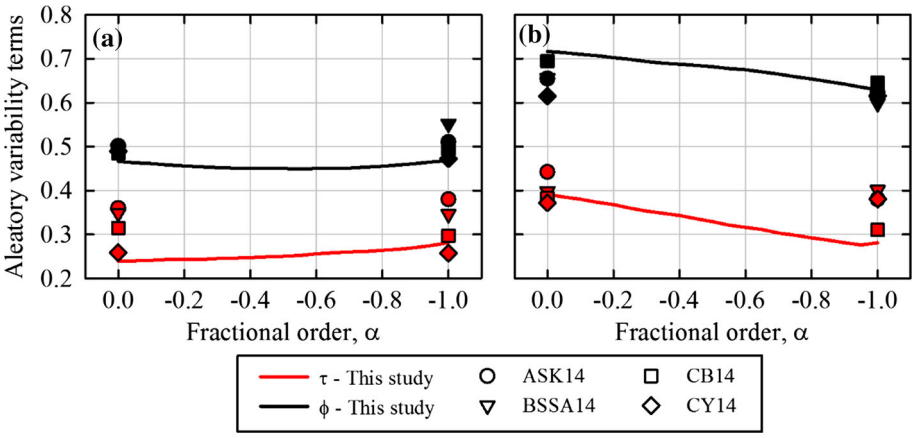

Fig. 17 Comparisons of aleatory variability components of the proposed predictive model with the NGA-West2 GMPEs: **a** $M_w = 7.5$ and $V_{S30} = 760$ m/s, **b** $M_w = 4.5$ and $V_{S30} = 255$ m/s

lower threshold magnitude, $M_w \sim 3.0$, than the predictive model in this study) between the proposed GMPE and NGA-West2 models.

8 Summary and conclusions

To develop a new ground-motion predictive model for a set of novel ground motion intensity measures—peak ground fractional order responses—a subset of the PEER NGA-West2 database is extracted by considering various inclusion criteria (e.g. only mainshock earthquakes from Western US; moment magnitude $M_w \geq 4.0$; extended-source distance metrics ≤ 300 km; known values of site class and style-of-faulting; well-recorded earthquakes with respect to minimum number of recordings criteria such as $N < 5$ for $M_w < 5.5$, $N < 3$ for $5.5 \leq M_w < 6.5$). The application of the above criteria results in the compilation of a ground-motion database with a total of 4491 recordings from 82 different earthquakes. Caputo's definition with modified Outsalup's recursive approximations in the frequency domain was used to compute the PGR_α values of the ground motion recordings.

The main functional form of the predictive model was selected by implementing rational data-driven testing tools from the literature, which compared alternative functional forms from the NGA-West2 predictive models. The final PGR_{α} GMPE accounts for magnitude, distance, style-of-faulting, linear and nonlinear site, hanging wall, basin response, and anelastic distance attenuation effects through the selected functional form. The site response and hanging wall effects of this predictive model were imported from the well-known models developed in the NGA-West2 project. To obtain the site response and hanging wall model coefficients that correspond to intermediate α values between PGA ($\alpha = 0$) and PGV ($\alpha = -1$), regression analyses were conducted. The final predictive model produces PGA ($\alpha = 0$), PGV ($\alpha = -1$), and peak ground fractional order responses at 19 α's ranging from -0.05 to -0.95.

Through the derivation of the newly proposed GMPE for PGR_{α}, insights are gleamed regarding the influence of various predictors (e.g. magnitude, distance, site effects) on the median value and aleatory variability of fractional order responses and how scaling effects vary as a function of α. For example, the fractional order scaling of the proposed GMPE exhibits different behaviors depending on magnitude level, and the soil nonlinearity effects are more pronounced with increasing level of spectral intensities. The resulting GMPE reveals high predictive quality across a range of fractional orders, while also taking care to account for various sources of aleatory variability. Given that predictive models of PGR_{α} are now available, and that existing work has suggested such fractional order IMs can provide more accurate predictions of the seismic response of structures, the outcomes of this study can enable utilization of a new class of ground motion intensity measures that take advantage of concepts of fractional order calculus for seismic risk assessment. On the other hand, there is still a strong need for work at the probabilistic seismic response level that compares optimal alpha level for a range of realistic structural systems and idealized/generalized cases. Future research should focus on investigation of fractional order IMs for a range of structural systems as well as exploration of the overall impact of integrating the proposed fractional order GMPE on resulting risk evaluations and loss estimates for distributed infrastructure systems. Beyond this, additional fractional order predictive models developed from different ground motion databases are needed to properly model the epistemic uncertainty in probabilistic seismic hazard analysis and to account for the regional variability while calculating the fractional order ground motion estimates.

9 Data and resources

This study uses a subset of the NGA-West 2 database (Ancheta et al. 2014). The flatfile and ground motion accelerograms can be accessed through the websites of NGA-West2 Project (http://peer.berkeley.edu/ngawest2/, last accessed June 2016) and PEER Ground Motion Database (http://ngawest2.berkeley.edu/, last accessed June 2016), respectively.

Acknowledgements The authors gratefully acknowledge the support of this research by the National Science Foundation of United States through Grants 1462177 and 1462183. The first author of this article was also supported by the Department of Science Fellowships and Grant Programs of the Scientific and Technological Research Council of Turkey (TUBITAK) for conducting his post-doctoral research studies at Rice University. Any opinions, findings and conclusions or recommendations expressed in this article are those of the authors and do not necessarily reflect the views of the sponsors. The authors thank Professors Sinan Akkar and M. Abdullah Sandıkkaya for providing random effects regression algorithms. The authors are also very grateful to two anonymous reviewers for their constructive feedback on the original version of this paper.

References

Abrahamson NA, Youngs RR (1992) A stable algorithm for regression analyses using the random effects model. Bull Seismol Soc Am 82:505–510

Abrahamson N, Silva W, Kamai R (2014) Summary of the ASK14 ground-motion relation for active crustal regions. Earthq Spectra 30:1025–1055

Akkar S, Kale Ö (2014) Reply to "Comment on 'A New Procedure for Selecting and Ranking Ground-Motion Prediction Equations (GMPEs): The Euclidean Distance-Based Ranking (EDR) Method' by Özkan Kale and Sinan Akkar" by Sum Mak, Robert Alan Clements and Danijel Schorlemmer. Bull Seismol Soc Am 104:3141–3144

Ancheta TD, Robert BD, Stewart PS, Seyhan E, Silva WJ, Chiou BSJ, Wooddell KE, Graves RW, Kottke AR, Boore DM, Kishida T, Donahue JL (2014) NGA-West 2 database. Earthq Spectra 30:989–1005

Bommer JJ, Stafford PJ, Alarcón JE, Akkar S (2007) The influence of magnitude range on empirical ground-motion prediction. Bull Seismol Soc Am 97:2152–2170

Bommer JJ, Douglas J, Scherbaum F, Cotton F, Bungum H, Fäh D (2010) On the selection of ground-motion prediction equations for seismic hazard analysis. Seismol Res Lett 81:783–793

Boore DM (2010) Orientation-independent, non geometric-mean measures of seismic intensity from two horizontal components of motion. Bull Seismol Soc Am 100:1830–1835

Boore DM, Stewart JP, Seyhan E, Atkinson GM (2014) NGA-West 2 equations for predicting PGA, PGV, and 5%-damped PSA for shallow crustal earthquakes. Earthq Spectra 30:1057–1085

Building Seismic Safety Council (BSSC) (2009) 2009 NEHRP recommended seismic provisions for new buildings and other structures: part 1, provisions. Federal Emergency Management Agency (P-750), Washington

Campbell KW, Bozorgnia Y (2014) NGA-West2 ground motion model for the average horizontal components of PGA, PGV, and 5%-damped linear acceleration response spectra. Earthq Spectra 30:1087–1115

Caponetto R (2010) Fractional order systems: modeling and control applications. World Scientific Publishing Company Incorporated, Singapore

Chang T, Singh MP (2002) Seismic analysis of structures with a fractional derivative model of viscoelastic dampers. Earthq Eng Eng Vib 1:251–260

Chiou BS-J, Youngs RR (2014) Update of the Chiou and Youngs NGA model for the average horizontal component of peak ground motion and response spectra. Earthq Spectra 30:1117–1153

Dikmen Ü (2005) Modeling of seismic wave attenuation in soil structures using fractional derivative scheme. J Balkan Geophys Soc 8:175–188

Donahue JL, Abrahamson NA (2014) Simulation-based hanging wall effects. Earthq Spectra 30:1269–1284

Gaul L, Klein P, Pienge M (1991) Simulation of wave propagation in irregular soil domains by BEM and associated small scale experiments. Eng Anal Bound Elem 8:200–205

Kaklamanos J, Baise LG, Boore DM (2011) Estimating unknown input parameters when implementing the NGA ground-motion prediction equations in engineering practice. Earthq Spectra 27:1219–1235

Kale Ö, Akkar S (2013) A new procedure for selecting and ranking ground-motion prediction equations (GMPEs): the Euclidean distance-based ranking (EDR) method. Bull Seismol Soc Am 103:1069–1084

Koh and Kelly (1990) Application of fractional derivatives to seismic analysis of base-isolated models. Earthquake Eng Struct 19:229–241

Lenti L, Nicolas JF, Bonilla F, Semblat JF, Martino S, Rovelli A (2012) Fractional derivatives: an alternative approach to model seismic wave attenuation and amplification. In: 15th World conference on earthquake engineering Sept 24–28, Lisbon, Portugal

Li HS, Luo Y, Chen YQ (2010a) A fractional order proportional and derivative (FOPD) motion controller: tuning rule and experiments. IEEE Trans Control Syst Technol 18:516–520

Li Y, Chen Y, Podlubny I (2010b) Stability of fractional-order nonlinear dynamic systems: Lyapunov direct method and generalized Mittag–Leffler stability. Comput Math Appl 59:1810–1821

Luco N, Cornell CA (2007) Structure-specific scalar intensity measures for near-source and ordinary earthquake ground motions. Earthq Spectra 23:357–392

Mackie K, Stojadinovic B (2001) Probabilistic seismic demand model for California highway bridges. J Bridge Eng 6:468–481

Mackie K, Stojadinovic B (2004) Improving probabilistic seismic demand models through refined intensity measures. In: 13th World conference on earthquake, Aug 1–6, Vancouver, Canada

Mainardi F (2010) Fractional calculus and waves in linear viscoelasticity: an introduction to mathematical models. World Scientific, Singapore

MathWorks (2015) MATLAB software. Natick, Massachusetts, United States of America

Meral F, Royston T, Magin R (2010) Fractional calculus in viscoelasticity: an experimental study. Commun Nonlinear Sci 15:939–945

Monje CA, Chen Y, Vinagre BM, Xue D, Feliu V (2010) Fractional-order systems and controls: fundamentals and applications. Springer, Berlin
Müller S, Kästner M, Brummund J, Ulbricht V (2011) A nonlinear fractional viscoelastic material model for polymers. Comput Mater Sci 50:2938–2949
Nash JE, Sutcliffe JV (1970) River flow forecasting through conceptual models: part I—a discussion of principles. J Hydrol 10:282–290
Odibat ZM (2010) Adaptive feedback control and synchronization of non-identical chaotic fractional order systems. Nonlinear Dyn 60:479–487
Oldham KB, Spanier J (1974) The fractional calculus: theory and applications of differentiation and integration to arbitrary order. Academic Press, San Diego
Oustaloup A, Levron F, Nanot F, Mathieu B (2000) Frequency-band complex non-integer differentiator: characterization and synthesis. IEEE Trans Circuits Syst I Fundam Theory Appl 47:25–39
Padgett JE, Nielson BG, DesRoches R (2008) Selection of optimal intensity measures in probabilistic seismic demand models of highway bridge portfolios. Earthquake Eng Struct 37:711–725
Podlubny I (1999) Fractional differential equations. Academic Press, New York
Ruge P, Trinks C (2004) Consistent modelling of infinite beams by fractional dynamics. Nonlinear Dyn 38:267–284
Scherbaum F, Cotton F, Smit P (2004) On the use of response spectral-reference data for the selection and ranking of ground-motion models for seismic-hazard analysis in regions of moderate seismicity: the case of rock motion. Bull Seismol Soc Am 94:2164–2185
Scherbaum F, Delavaud E, Riggelsen C (2009) Model selection in seismic hazard analysis: an information-theoretic perspective. Bull Seismol Soc Am 99:3234–3247
Shafieezadeh A, Ramanathan K, Padgett JE, DesRoches R (2012) Fractional order intensity measures for probabilistic seismic demand modeling applied to highway bridges. Earthq Eng Struct 41:391–409
Singh MP, Chang T-S, Nandan H (2011) Algorithms for seismic analysis of MDOF systems with fractional derivatives. Eng Struct 33:2371–2381
Tavazoei MS, Haeri M (2008) Chaos control via a simple fractional-order controller. Phys Lett A 372:798–807
Xue D, Zhao C, Chen Y (2006) A modified approximation method of fractional order system. In: 2006 IEEE international conference on mechatronics and automation, June 25–28, Luoyang, China